



UNIVERSITY OF LEEDS

This is a repository copy of *Modeling a halogen dance reaction mechanism: A density functional theory study*.

White Rose Research Online URL for this paper:

<https://eprints.whiterose.ac.uk/97279/>

Version: Accepted Version

Article:

Jones, L and Whitaker, BJ (2016) Modeling a halogen dance reaction mechanism: A density functional theory study. *Journal of Computational Chemistry*, 37 (18). pp. 1697-1703. ISSN 0192-8651

<https://doi.org/10.1002/jcc.24385>

© 2016 Wiley Periodicals, Inc. This is the peer reviewed version of the following article: Jones, L and Whitaker, BJ (2016) Modeling a halogen dance reaction mechanism: A density functional theory study. *Journal of Computational Chemistry*, 37 (18). pp. 1697-1703, which has been published in final form at <http://dx.doi.org/10.1002/jcc.24385>. This article may be used for non-commercial purposes in accordance with Wiley Terms and Conditions for Self-Archiving. Uploaded in accordance with the publisher's self-archiving policy.

Reuse

Items deposited in White Rose Research Online are protected by copyright, with all rights reserved unless indicated otherwise. They may be downloaded and/or printed for private study, or other acts as permitted by national copyright laws. The publisher or other rights holders may allow further reproduction and re-use of the full text version. This is indicated by the licence information on the White Rose Research Online record for the item.

Takedown

If you consider content in White Rose Research Online to be in breach of UK law, please notify us by emailing eprints@whiterose.ac.uk including the URL of the record and the reason for the withdrawal request.



eprints@whiterose.ac.uk
<https://eprints.whiterose.ac.uk/>

Modeling a Halogen Dance (HD) Reaction Mechanism: A Density Functional Theory (DFT) Study

Leighton Jones¹ and Benjamin J. Whitaker¹,

Correspondence to: Benjamin J. Whitaker (E-mail: B.J.Whitaker@leeds.ac.uk)

¹School of Chemistry, University of Leeds, Leeds, LS2 9JT UK

ABSTRACT

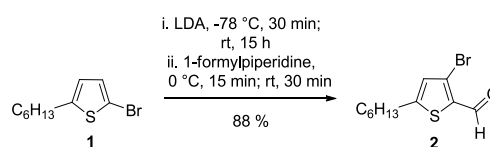
Since the discovery of the halogen dance (HD) reaction more than sixty years ago, numerous insights into the mechanism have been unveiled. To date however, the reaction has not been investigated from a theoretical perspective. Density functional theory (DFT) was used to model the potential energy surface (PES) linking the starting reagents to the lithiated products for each step in the mechanism using a thiophene substrate. It was found that the lithium-halogen exchange mechanism is critical to understand the HD mechanism in detail and yielded the knowledge that S_N2 transition states are favoured over the four-centre type for the lithium-bromine exchange steps. The overall driving force for the HD is thermodynamics, while the kinetic factors tightly control the reaction path through temperature. The S_N2 lithium-bromide transition states are barrierless, except the second which is the limiting step. Finally, the model for the HD is discovered to be a pseudo-clock type, due to a highly favourable bromide catalysis step and the reformation of 2-bromothiophene.

Introduction

Halogen dance (HD) reactions are intermolecular rearrangements of halogen substituents on aromatic rings. The reaction class is a useful tool in the synthesis of materials for a range of applications from organic semiconductors to chiral drug scaffolds¹⁻⁵. HD reactions have been observed for diverse substrates including thiophene^{6, 7}, phenyl^{8, 9}, furan^{10, 11}, thiazole¹², oxazole¹³ and pyridine¹⁴ units.

As an example, whose detailed mechanism we explore with density functional theory (DFT) below, Scheme 1 illustrates the HD reaction with 2-bromo-5-hexylthiophene (**1**) and LDA affording 3-bromo-2-formyl-5-hexylthiophene (**2**) in 88% yield¹⁵. The reaction shows the repositioning of the bromine atom on the thiophene ring and the addition of a formyl transfer agent, 1-formylpiperidine, immediately quenching the lithium salt and yielding the target **2**. This scheme illustrates how the HD reaction can generate a useful bi-functional product in

high yield from a mono-functional starting reagent.



Scheme 1. The Synthesis of the HD mediated 3-bromo-2-formyl-5-hexylthiophene product.

The base which led to the discovery of the HD reaction (in 1951) was sodium acetylide in liquid ammonia¹⁶. The generality of the reaction was confirmed two years later by the same research group using sodium amide⁷. For these reactions mixtures of polybrominated species were observed in the products. Subsequent work using bases such as potassium anilide⁶ and lithium diisopropylamine (LDA)¹⁵ has, however, shown that the conditions of the HD reaction can be adjusted to produce a relatively clean product.

The conditions of the reaction are typically low temperatures (-78 °C) for a short time (30 min), after which the mixture is allowed to warm to room temperature and stirred overnight. These conditions are 'promotive' of an HD reaction¹⁷, but give little indication as to the likely mechanism.

Proposed mechanisms have been difficult to test because the multiple intermediates are highly reactive and hard to observe directly. However, infrared absorption spectroscopy has been used to monitor organolithium intermediates in cryogenic reactors¹⁸. Very fast rates were observed for the lithiation of 2- and 3-bromothiophene by LDA in THF at -86 °C, in which a steady state was reached within *ca.* a minute. The relatively faster reaction of the 3-bromo compound was attributed to a stronger inductive effect of the bromine substituent compared to 2-bromothiophene (no reaction was observed for thiophene at -86 °C although metallation was observed at -40 °C). IR absorption cannot be applied to follow the subsequent steps of the HD as the spectral profiles of the species under investigation overlap. To the best of our knowledge, our work is the first attempt to follow each step of the halogen dance through the use of quantum chemistry modelling.

Methods

Computational Methods

All calculations were performed with the Gaussian 09 software package¹⁹ at various levels of approximation. The basis set 6-311++G(d,p) was used for the majority of calculations. The addition of diffuse functions in the basis set was helpful to describe the long range dipole-dipole interactions in the initial steps of the reaction. Although we attempted some calculations at the CCSD level of theory these were computationally too expensive for the exploration of the global potential energy landscape and most of the

calculations reported below were performed using density functional theory (DFT) with the Becke-3 parameter density functional and the Lee–Yang–Parr correlation functional (B3LYP).

Initial calculations found the long range correction to DFT, Coulomb-attenuating method (CAM-B3LYP), made relatively little or no difference to the recovered activation energies or energy profiles and all subsequent calculations were performed at the B3LYP level. Dispersion functionals later applied included Grimme's D2 term²⁰, Becke-Johnson damping²¹ and wB97XD²². Stationary points on the potential energy surface (PES) were obtained using the synchronous transit-guided quasi-Newton (STQN) method and the QST3 keyword; that is by specifying an intermediate molecule presumed to be close to the transition state (TS) in addition to the previously optimized structures of the reactants and products. The stationary nature of the TSs was in each case confirmed by subsequent frequency and intrinsic reaction coordinate (IRC) path following calculations. The IRC calculations were performed in vacuum.

Thermodynamic quantities (Gibbs free energies) were calculated at 1 atm and 298 K from frequency calculations and then corrected to account for the difference between the standard state in the gas phase and solution (1 atm vs 1 M) by adding $RT\ln(24.46)$.

The solution phase was investigated using a variety of methods ranging from continuum models such as the integral equation formalism polarisable continuum model (IEFPCM), a variant (SMD) and the conductor polarisable continuum model (CPCM), to the calculation of explicit solvent molecules imbedded in a continuum.

To simplify the modelling of the reaction described in Scheme 2, the LDA is replaced by lithium amide (LiNH₂) and the 2-bromo-5-hexylthiophene is replaced by 2-bromothiophene in the model.

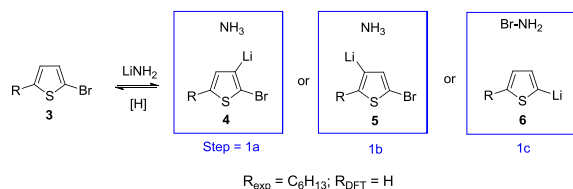
Synthesis of 3-bromo-2-formyl-5-hexylthiophene

N-butyl lithium (18.3 mL, 29.2 mmol, 1.6 M in hexane) was added to a stirred solution of diisopropylamine (5.11 mL, 36.5 mmol) in tetrahydrofuran (120 mL) at $-78\text{ }^{\circ}\text{C}$. The mixture was stirred for 15 min, then allowed to warm to $0\text{ }^{\circ}\text{C}$ for 15 min. 2-bromo-5-hexylthiophene (6.00 g, 24.3 mmol) was added to the reaction mixture at $-78\text{ }^{\circ}\text{C}$ and stirred for 30 min, then allowed to warm to room temperature for 15 h. The mixture was quenched with 1-formylpiperidine (3.78 mL, 34.0 mmol) at $0\text{ }^{\circ}\text{C}$ and stirred for 15 min, then stirred at room temperature for 30 min. The mixture was extracted with diethyl ether (25 mL \times 4), dried over sodium sulfate and the solvent removed giving a crude brown oil. The crude was purified over silica in petroleum ether ($40\text{--}60\text{ }^{\circ}\text{C}$) and dichloromethane (1:1) affording an orange oil, 5.92 g, 21.5 mmol, 88 % yield; δ_{H} (500 MHz, CDCl_3): 9.91 (s, 1H), 6.88 (s, 1H), 2.86 (t, 2H, $J = 7.7$), 1.71 (q, 2H, $J = 7.35, 7.49$), 1.37 (m, 6H), 0.92 (t, 3H, $J = 6.9$); δ_{C} (500 MHz, CDCl_3): 182.7, 157.1, 134.5, 129.3, 120.3, 31.4, 30.9, 30.8, 26.6, 22.5, 14.0; (EI+): 274.0020; micro calc. C 48.01, H 5.49, S 11.65, Br 29.03, found C 46.80, H 5.40, S 11.60, Br 29.20.

Results and Discussion

As we describe below, we are able to locate and characterize transition states and intermediates connecting **1** and **2** and in so doing describe the kinetic and thermodynamic controls governing this HD reaction.

The mechanism behind the HD reaction is generally believed to consist of a cascade of deprotonation (metal-hydrogen exchange) and metal-halogen exchange reactions¹⁷. Scheme 2 shows the possible first steps, as they might apply to the synthesis of 3-bromo-2-formyl-5-hexylthiophene. In the model we only consider the lithiation and bromination possibilities for the 2, 3 and 4 positions around thiophene because in the



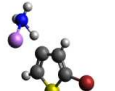
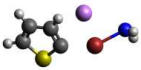
Scheme 2. Lithiation of 2-bromothiophene. The possible products of each of the reactions are labelled **4**, **5**, and **6**, and the associated reactions as step 1a, 1b and 1c respectively.

“real” chemistry the 5 position is blocked by alkyl chains or other derivatives (see Scheme 1). We label the proton abstraction of 2-bromothiophene (**3**) at the 3 (**4**) or 4 positions (**5**), or lithium halogen exchange at the 2 position (**6**), as steps 1a, 1b and 1c respectively.

Chemical intuition would suggest that the proton at position 3 would be the most easily removed. This is confirmed by calculating the Gibbs energies of the respective anions in THF using the default polarizable continuum model. At the B3LYP/6-311++G(d,p) level we find, as expected, the Gibbs free energy of the anion deprotonated at position 3 is lower than the other two positions, and hence the proton at this position would be preferentially abstracted. This conclusion is confirmed with pKa and atomic charge analysis (see supporting information).

While it is known that reagents like alkyl lithium aggregate, there is uncertainty with regards to the degree²³. pKas and lithium equilibria have been investigated by Streitwieser²⁴ who found that solvation continuum models were inadequate for the study of lithiated species (in THF), which are believed to exist as tetramers at low temperatures in solution. On the other hand NMR studies²⁵ find the binding of explicit solvent molecules to lithiated reagents is under kinetic rather than thermodynamic control. It is also known that there are large interaction energies associated with ethers which may determine the degree of aggregation²⁶. Due to the uncertainty over aggregation, we begin our investigations by considering undissociated lithium reagents and monomeric species in vacuum.

The results for the lithiation possibilities of the first step are summarized in Table 1 (see supporting information for structural data); the frequencies correlate well with phenyl lithium-proton stretches²⁷. The barrier of 1a is the smallest (9.81 kJ mol⁻¹) while 1c is the largest.

Table 1. Transition states ^a , frequencies, activation energies and Gibbs reaction energies for steps 1a-c.				
Step	TS [‡]	Vibration / cm ⁻¹	U _a / kJ mol ⁻¹	Δ _r G / kJ mol ⁻¹
1a		1325 <i>i</i>	9.81	22.51
1b		1366 <i>i</i>	30.26	51.05
1c		229.1 <i>i</i>	110.11	115.53

[a] Computed at the B3LYP/6-311++G(d,p) level.

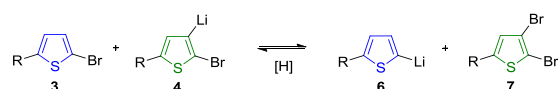
Having located the transition states for the three possibilities of the first step of the dance, we then calculated the reaction energy profiles along their IRCs. Due to the deep dipole-dipole wells in both the entrance and exit channels we were unable to follow the reaction to completion in either direction. The IRC paths 1a-c are referenced to the sum of the energy of the individually optimised reagents, shown as the filled triangle (labelled 1a OR) on the left hand side of Figure 1. The sum of energies of the individually optimised products for the three reactions is shown on the right hand side of the diagram.

The striking difference between the lithium-hydrogen exchange reactions and the lithium-halogen exchange reaction is the nature of their transition states. Both reaction steps 1a and 1b have tight transition states, while 1c is relatively loose. All three reactions exhibit deep wells in both entrance and exit channels. These are due

to dipole-dipole interactions between the reactants and products. For both lithium-halogen exchange reactions the well on the product side is significantly more stable than that on the reactant side, so despite the fact that reactions 1a and 1b are both predicted to be endothermic (Δ_rU_g of +20.4 and +49.7 kJ mol⁻¹ respectively) the complex on the product side is predicted to be thermodynamically favoured.

Both lithium-hydrogen exchange reactions 1a and 1b have modest barriers in the forward direction, *ca.* 10 kJ mol⁻¹ and 30 kJ mol⁻¹ respectively. At -78 °C reaction 1a is expected to be kinetically favoured over 1b by a factor of order 2.3×10⁵. However, the reaction rate at low temperature may also be enhanced by quantum mechanical tunnelling through the narrow barrier between the entrance and exit channel complexes. Thus the most likely product of the first step of the dance is a lithium-proton exchange reaction, probably favouring the production of 3-lithio-2-bromothiophene (**4**) over 4-lithio-2-bromothiophene (**5**).

We now need to consider the reactions of step 2, the lithium-halogen exchange between **3** and **4** as shown in Scheme 3. While **6** was found to be kinetically and thermodynamically unfavourable from the reaction of **3** and lithium amide, **6** has now to be produced from the forward reaction step 2.



Scheme 3. Reaction step 2, the generation of the 2,3-dibromothiophene **7**; the colours indicate the substrate transformation.

Species **6** and **7** must then undergo a transmetalation between the thiophene partners (Scheme 4) to produce the target lithium species **8**. To achieve this, the lithium and bromine atoms of **6** and **7** exchange places thereby reforming the starting reagent **3**; we call this a “do-si-do” reaction after the basic dance step commonly known in square dancing. The

reformation of **3** suggests the overall mechanism is autocatalytic or pseudo-clock type.

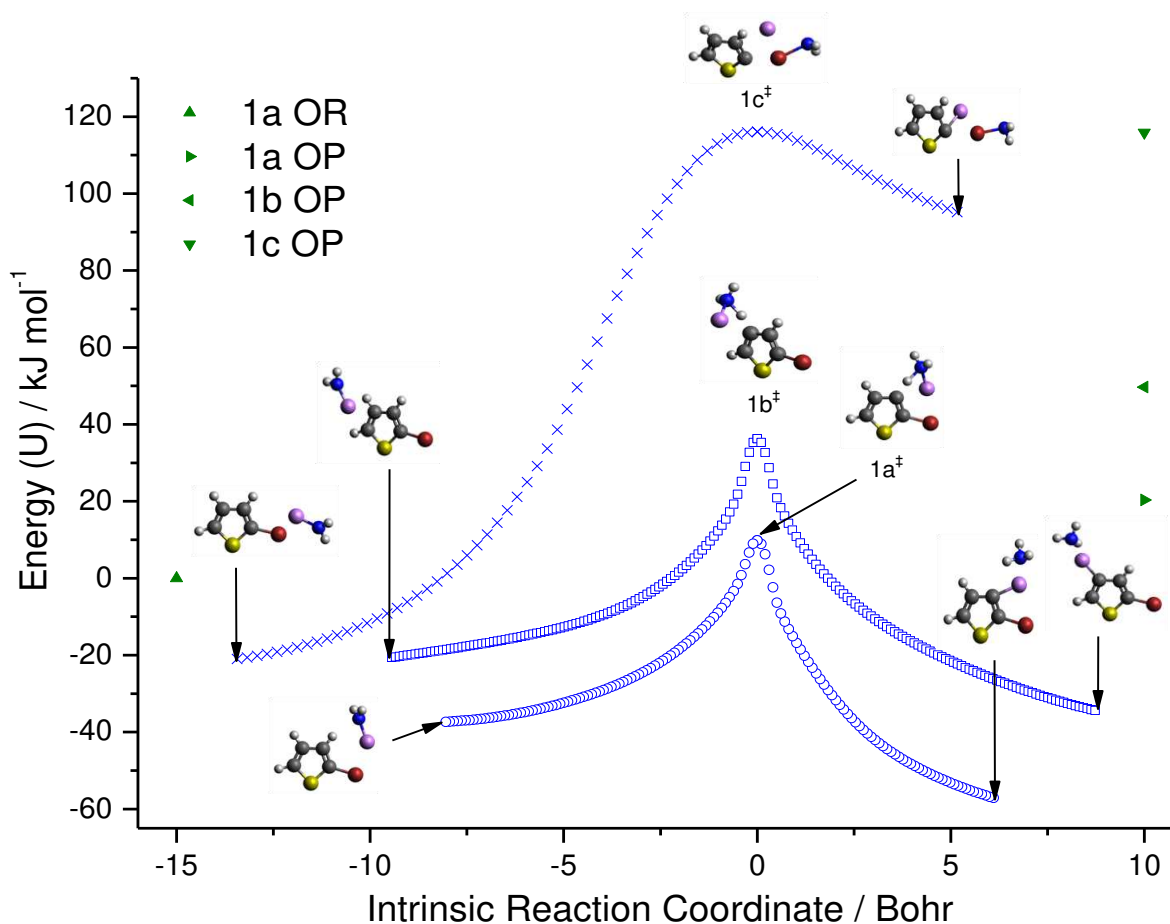
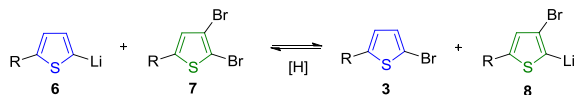


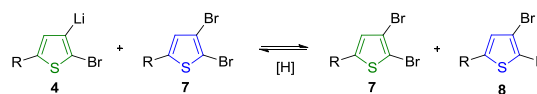
Figure 1. Minimum energy path along the forward and reverse intrinsic reaction coordinates of steps 1a-c, relative to the energy of the starting materials; the optimised reagents (OR) and optimised products (OP) are shown as single data points (green triangles). The potential energy wells in the entrance and exit channels are due to strong dipole-dipole interactions between the reactants and products; 1a has deeper potential energy wells than 1b or 1c due to a dipole alignment at the 3 position of thiophene.



Scheme 4. Reaction step 3, the “do-si-do”; the colours indicate the substrate transformation.

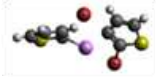
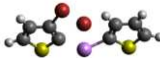
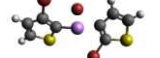
To complicate matters, it is possible for reagent **4** and product **7** species from step 2 to cross couple and undergo their own lithium-halogen exchange to furnish an alternative or bromide catalysis, also giving **8** (Scheme 5). If this were the case, it must be an

additional step (step 4), only possible once some 2,3-dibromothiophene (**7**) has been formed from step 2. Since **7** is both a reagent and product it could also be influential in the HD as an auto catalyst.



Scheme 5. Bromide catalysis (step 4), generating major lithium species **8**; the colours indicate the substrate transformation.

We were able to locate four-centre type transition states for the lithium-halogen exchange steps 2, 3 and 4 *via* the STQN method and confirm their stationary nature with frequency and IRC calculations (see supporting information), summarized in Table 2. Step 2 is only slightly endothermic ($11.05 \text{ kJ mol}^{-1}$) but is predicted to proceed over a substantial barrier of $202.2 \text{ kJ mol}^{-1}$. Steps 3 and 4 have similarly high barriers but are exothermic (-49.3 and $-38.3 \text{ kJ mol}^{-1}$ respectively). The transmetalation of lithium between the two thiophenes in the transition states appears to occur by a cradle-like structure, as illustrated in Figure 2.

Table 2. Transition states (four-centre type), frequencies, activation energies and Gibbs reaction energies for steps 2-4.				
Step	TS [‡]	Vibration / cm^{-1}	$U_a / \text{kJ mol}^{-1}$	$\Delta_r G / \text{kJ mol}^{-1}$
2		265.0i	202.2	11.05
3		266.2i	175.6	-49.29
4		272.5i	193.1	-38.25

[a] Computed at the B3LYP/6-311++G(d,p) level

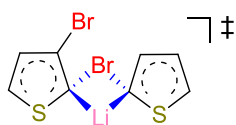


Figure 2. The four-centre geometry of the lithium-halogen exchange transition state 3; the lithium atom is directly bound to both carbanions.

The relatively large energy barriers in the reverse direction and the deeper energy wells on the product side of steps 3 and 4 essentially traps the target lithium species **8**. The build-up of **8** over time ensures **11** is produced as the major product upon quenching with an electrophile.

Thus far we have uncovered the rearrangement of lithium, proton and bromine

atoms on a thiophene substrate, linking the suspected steps in the halogen-dance mechanism through four-centre type lithium-bromine exchange steps. Yet the activation energies presented from these studies suggest each reaction step to be improbable, even at room temperature. We therefore attempted to improve the model by (1) long range correction to the potentials, swapping B3LYP for LC-wPBE²⁸ and LC-BLYP, (2) dispersion-corrected functionals²⁰, and (3) explicit and continuum solvation models²⁹ of THF.

Long-range corrected functionals gave four-centre type transition states with single imaginary frequencies, but only at the lower basis set of 6-31+G(d). Grimme's dispersion-corrected functionals resulted in transition states (confirmed with IRC calculations) that gave the expected reagents and products at the B3LYP/6-311++G(d,p) level. The resulting activation energies were reduced by 30-40 kJ mol^{-1} , in comparison to the non-dispersion corrected functionals (activation energies for all steps at different levels of theory are tabulated in the supporting information). The overall result, however, is that while the barriers are somewhat lower when dispersion terms are considered, the resultant barrier heights are still far too high to be consistent with experiment.

Post-HF calculations of the transition states proved to be computationally intractable, but we were able to investigate the thermodynamics at the MP2 and CCSD levels of theory. CCSD gives almost identical endo- and exothermicities to the B3LYP-D3BJ and D2 functionals (*i.e.* to within chemical accuracy of *ca.* 3 kJ mol^{-1}).

Even though dispersion-corrected functionals give a significant improvement, the activation energies for steps 3 and 4 remain high. We therefore attempted to improve the calculations using an explicit solvation model, using steps 1a and 2 as suitable test-case transition states (Table 3). An explicit THF molecule coordinated to the lithium atom (calculated in vacuum)

increases the barrier heights by ~ 9 and ~ 21 kJ mol^{-1} respectively. This suggests, that adding electron density to the lithium atom weakens the lithium-carbon bonds and destabilises the transition state. Although Streightweiser²⁴ suggests explicit solvation models to be the most appropriate, continuum

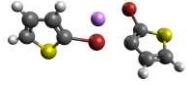
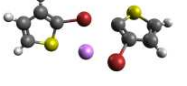
Step	THF ^a	IEFPCM ^b	SMD ^c	CPCM ^d
1a	18.59	26.15	18.47	25.96
2	222.9	215.5	195.5	215.1

[a] Explicit THF molecule, [b] the default Integral Equation Formalism Polarizable Continuum Model (IEFPCM) in G09, [c] Truhlar's and co-workers solvation model incorporating electron density (SMD), [d] Conductor Polarizable Continuum Model (CPCM); [a] is at the B3LYP/6-311++G(d,p) and [b-d] is B3LYP-D2/6-311++G(d,p) levels

models were also investigated, namely the default Integral Equation Formalism Polarizable Continuum Model (IEFPCM)²⁹ in G09, Truhlar's and co-workers solvation model incorporating electron density (SMD)³⁰ which is a variant of IEFPCM and the Conductor Polarizable Continuum Model (CPCM)³¹. It was found that all of these models increased the barriers by varying degrees (of order 10-25 kJ mol^{-1}).

It is clear that solvation models (explicit and continuum) do not explain how the reaction can proceed smoothly in THF because the predicted activation barriers are large and kinetically unfavourable. This suggests that an alternative lithium-halogen exchange mechanism needs investigating to locate reasonable energy barriers for the HD reaction. Multiple attempts at locating a 'bromate' type transition state were not successful as they also resulted in the formation of bithiophene products and the release of lithium bromide - clearly incorrect. Alternatively, S_N2 type transition states were investigated. Such transition states were found for all the lithium-halogen exchange steps 2-4, with a single imaginary frequency each (Table 4) and confirmed with IRC calculations. The S_N2 transition states show the lithium coordinated in between the bromine atoms (Figure 3) and the

sulfur of the thiophene (step 3). The barrier for step 2 is reduced from *ca.* 200 to 45 kJ mol^{-1} , and steps 3 and 4 become barrierless (-12.22 and -20.89 kJ mol^{-1}), where 4 is the most favourable reaction.

Step	TS [‡]	Vibration / cm^{-1}	$U_a / \text{kJ mol}^{-1}$
2		112.7 <i>i</i>	44.93
3		143.4 <i>i</i>	-12.22
4		72.35 <i>i</i>	-20.89

[a] Calculated at the B3LYP-D2/6-311++G(d,p) level.

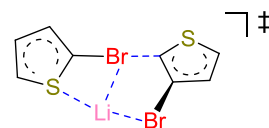


Figure 3. The S_N2 geometry of the lithium-halogen exchange transition state 3; the lithium atom coordinates between the bromine atoms (and partially to sulfur with state 3).

The overall Gibbs energy profile for the S_N2 mechanism is illustrated in Figures 4 and 5 for steps 2-3 and 4 respectively (the corresponding Gibbs energy profiles for the four-centre type are in the supporting information). Figure 4 suggests that step 2, proceeding *via* an S_N2 type transition state, is the rate determining step in the halogen dance reaction. As shown in the supporting information, the minimum energy paths also all exhibit deep wells on both sides of the transition state for all the S_N2 type reactions. Reactions 3 and 4 show 'submerged' transition states which lie below the energies of the optimised starting materials, but flanked on either side by deep attractive wells due to the dipole-dipole interactions between both the reactant and product species. This suggests that the entire reaction sequence from the initial

lithiation step to the halogen exchange occurs between the same sets of molecules which are

strongly confined by the electrostatic forces between them.

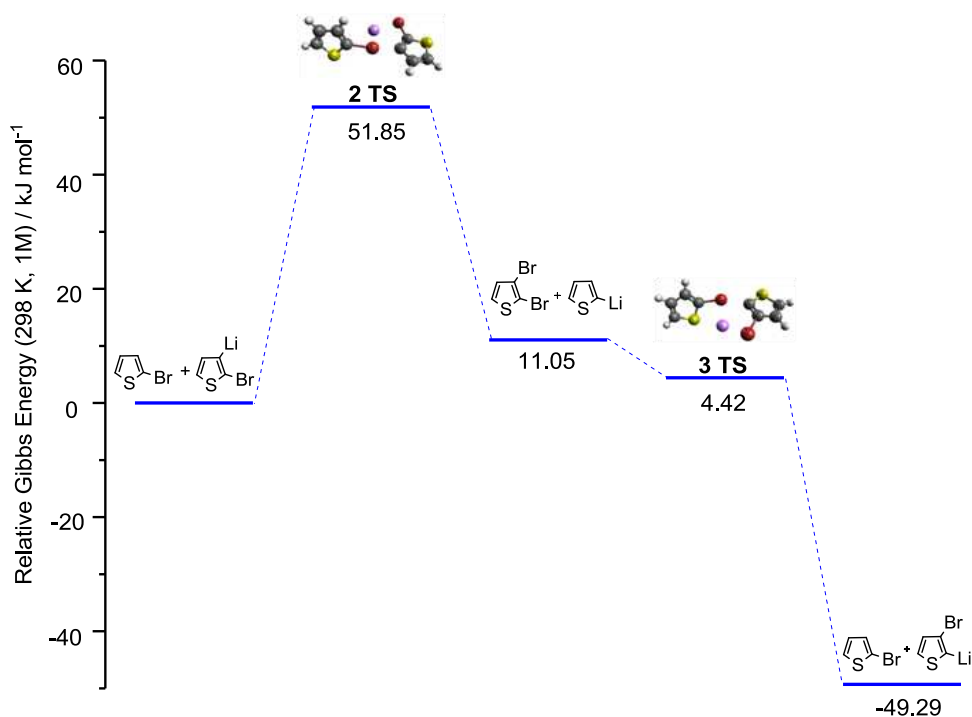


Figure 4. The relative Gibbs energy profile for the S_N2 mechanism steps 2 and 3. For clarity, the wells in the entrance and exit channels are not shown.

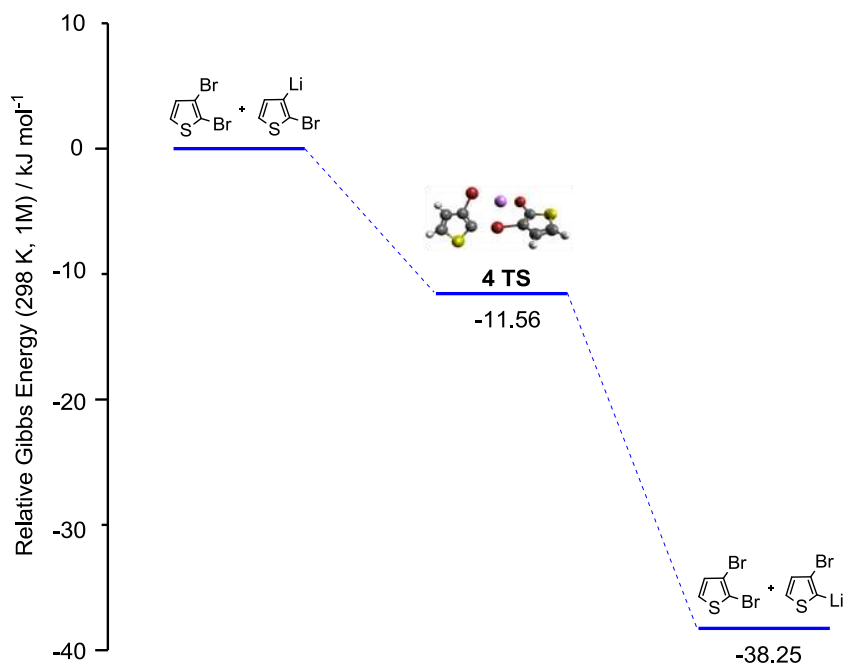
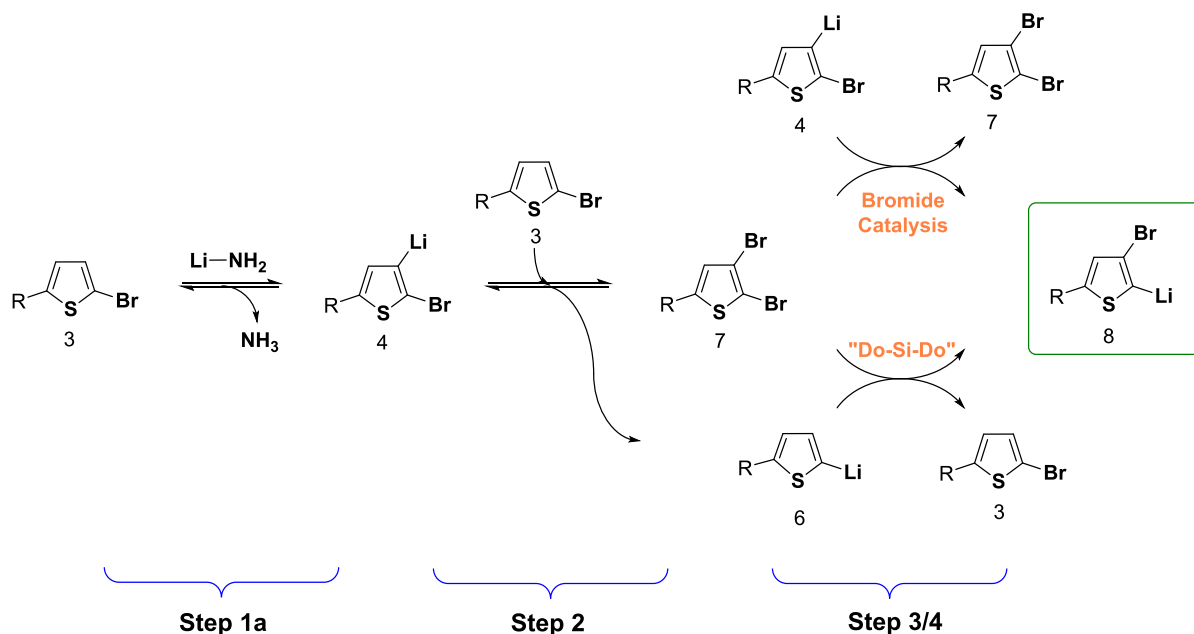


Figure 5. The relative Gibbs energy profile for the S_N2 mechanism step 4. For clarity, the wells in the entrance and exit channels are not shown.

A plausible mechanism, similar to that proposed in the literature¹⁵, for the model halogen dance reaction is outlined in Scheme 6. One proton abstraction at the 3 position and two lithium-halogen exchanges can afford the target lithium species (**8**) in just three steps. Step 2 is predicted to be the rate limiting step with a barrier of *ca.* 45 kJ mol⁻¹. Steps 3 and 4 are predicted to be barrierless with submerged

transition states (*i.e.* exhibit negative barriers with potential wells in the entrance and exit channels). This conclusion is consistent with the two key requirements for the HD reaction originally outlined by Frohlich¹⁵, that (a) the HD reaction is promoted by base and (b) the formation of 2,3-dibromothiophene is needed.



Scheme 6. A plausible mechanism for the model HD reaction; $\text{R}=\text{C}_6\text{H}_{13}$ experimentally and $\text{R}=\text{H}$ in model.

Conclusions

Using DFT we have investigated the potential energy landscape of a model Halogen Dance reaction and have located and characterized two types of transition state, four-centre and $\text{S}_{\text{N}}2$ type, for the lithium-halogen exchange which is central to the Halogen Dance mechanism.

The four-centre transition state is found to lead to activation barriers which are inconsistent with experimental observation that the reaction proceeds smoothly and quite rapidly at room temperature after the initial low temperature lithiation of the halogenated substrate. The rate determining step is the reaction of the substrate with lithiated product to generate a 2,3-dibromothiophene *via* an $\text{S}_{\text{N}}2$ type transition state. The 2,3-dibromothiophene subsequently reacts with lithiated product *via* two barrierless paths, connected by submerged $\text{S}_{\text{N}}2$ type transition states, leading to exchange of the halogen and lithium substituents.

Our conclusions, of course, depend on the accuracy of the model chemistry. In this respect

it is known that although hybrid DFT methods, which mix Hartree-Fock theory with Kohn-Sham DFT, such as B3LYP, perform better than pure DFT methods, they have been optimized against thermochemistry data sets only and are known to systematically underpredict barrier heights. By calibration against a database of barrier heights for 19 non-hydrogen transfer reactions, Truhlar and co-workers estimate a mean unsigned error of *ca.* 18 kJ mol^{-1} in barrier height compared to experiment³². Although this is a chemically significant error it will not affect the main mechanistic conclusions of our calculations since the difference in the barrier heights of the two mechanisms differ by more than the expected errors.

The main driving force is thermodynamic, but the most likely reaction path is revealed from the kinetic considerations detailed in this work. While dibromothiophenes may act to catalyse the reaction, the reformation of 2-bromothiophene suggests the HD reaction of 5-alkyl-2-bromothiophene is a pseudo-clock type.

Acknowledgements

LJ is grateful to the Gunnell and Matthews Scholarship for financial support. We are grateful to a referee for pointing out the deficiencies of the B3LYP methodology with respect to the calculation of transition state energies.

Keywords: Density functional calculations, aromatic substitution, transition states, molecular modelling

(Additional Supporting Information can be found in the online version of this article.)

References and Notes

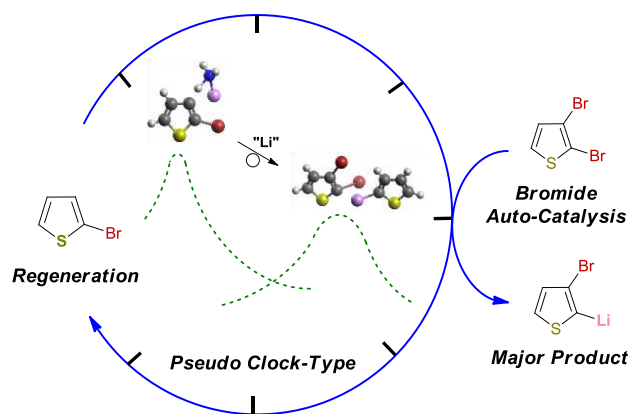
1. M. Ashizawa, T. Niimura, Y. Yu, K. Tsuboi, H. Matsumoto, R. Yamada, S. Kawauchi, A. Tanioka and T. Mori, *Tetrahedron*, 2012, **68**, 2790-2798.
2. J. L. Brusso, O. D. Hirst, A. Dadvand, S. Ganesan, F. Cicoira, C. M. Robertson, R. T. Oakley, F. Rosei and D. F. Perepichkat, *Chemistry of Materials*, 2008, **20**, 2484-2494.
3. S. Y. Kang, K. S. Song, J. Lee, S. H. Lee and J. Lee, *Bioorganic & Medicinal Chemistry*, 2010, **18**, 6069-6079.
4. M. Ohtawa, S. Ogihara, K. Sugiyama, K. Shiomi, Y. Harigaya, T. Nagamitsu and S. Omura, *Journal of Antibiotics*, 2009, **62**, 289-294.
5. P. Schuisky, H. J. Federsel and W. Tian, *Journal of Organic Chemistry*, 2012, **77**, 5503-5514.
6. C. E. Moyer and J. F. Bunnett, *Journal of the American Chemical Society*, 1963, **85**, 1891-&.
7. A. Vaitiekunas and F. F. Nord, *Journal of the American Chemical Society*, 1953, **75**, 1764-1768.
8. X. F. Duan and Z. B. Zhang, *Heterocycles*, 2005, **65**, 2005-2012.
9. T. Kojima and S. Hiraoka, *Organic Letters*, 2014, **16**, 1024-1027.
10. J. Frohlich and C. Hametner, *Monatshefte Fur Chemie*, 1996, **127**, 435-443.
11. J. Frohlich, F. Sauter and K. Blasl, *Heterocycles*, 1994, **37**, 1879-1891.
12. E. L. Stangeland and T. Sammakia, *Journal of Organic Chemistry*, 2004, **69**, 2381-2385.
13. P. Stanetty, M. Spina and M. D. Mihovilovic, *Synlett*, 2005, 1433-1434.
14. M. J. Pieterse and H. J. Denhertog, *Recueil Des Travaux Chimiques Des Pays-Bas-Journal of the Royal Netherlands Chemical Society*, 1962, **81**, 855-&.
15. J. Frohlich, C. Hametner and W. Kalt, *Monatshefte Fur Chemie*, 1996, **127**, 325-330.
16. A. Vaitiekunas and F. F. Nord, *Nature*, 1951, **168**, 875-876.
17. M. Schnurch, M. Spina, A. F. Khan, M. D. Mihovilovic and P. Stanetty, *Chemical Society Reviews*, 2007, **36**, 1046-1057.
18. D. Lumpi, C. Wagner, M. Schopf, E. Horkel, G. Ramer, B. Lendl and J. Frohlich, *Chemical Communications*, 2012, **48**, 2451-2453.
19. M. J. T. Frisch, G. W.; Schlegel, H. B.; Scuseria, G. E.; Robb, M. A.; Cheeseman, J. R.; Scalmani, G.; Barone, V.; Mennucci, B.; Petersson, G. A.; Nakatsuji, H.; Caricato, M.; Li, X.; Hratchian, H. P.; Izmaylov, A. F.; Bloino, J.; Zheng, G.; Sonnenberg, J. L.; Hada, M.; Ehara, M.; Toyota, K.; Fukuda, R.; Hasegawa, J.; Ishida, M.; Nakajima, T.; Honda, Y.; Kitao, O.; Nakai, H.; Vreven, T.; Montgomery, J. A., Jr.; Peralta, J. E.; Ogliaro, F.; Bearpark, M.; Heyd, J. J.; Brothers, E.; Kudin, K. N.; Staroverov, V. N.; Kobayashi, R.; Normand, J.; Raghavachari, K.; Rendell, A.; Burant, J. C.; Iyengar, S. S.; Tomasi, J.; Cossi, M.; Rega, N.; Millam, J. M.; Klene, M.; Knox,

- J. E.; Cross, J. B.; Bakken, V.; Adamo, C.; Jaramillo, J.; Gomperts, R.; Stratmann, R. E.; Yazyev, O.; Austin, A. J.; Cammi, R.; Pomelli, C.; Ochterski, J. W.; Martin, R. L.; Morokuma, K.; Zakrzewski, V. G.; Voth, G. A.; Salvador, P.; Dannenberg, J. J.; Dapprich, S.; Daniels, A. D.; Farkas, Ö.; Foresman, J. B.; Ortiz, J. V.; Cioslowski, J.; Fox, D. J., Gaussian Inc., Wallingford CT, 2009.
20. S. Grimme, *Journal of Computational Chemistry*, 2006, **27**, 1787-1799.
21. S. Grimme, S. Ehrlich and L. Goerigk, *Journal of Computational Chemistry*, 2011, **32**, 1456-1465.
22. J.-D. Chai and M. Head-Gordon, *Physical Chemistry Chemical Physics*, 2008, **10**, 6615-6620.
23. G. Fraenkel, S. Subramanian and A. Chow, *Journal of the American Chemical Society*, 1995, **117**, 6300-6307.
24. A. Streitwieser, J. R. Reyes, T. Singhapricha, S. Vu and K. Shah, *The Journal of Organic Chemistry*, 2010, **75**, 3821-3830.
25. A. Corruble, D. Davoust, S. Desjardins, C. Fressigné, C. Giessner-Prettre, A. Harrison-Marchand, H. Houte, M.-C. Lasne, J. Maddaluno, H. Oulyadi and J.-Y. Valnot, *Journal of the American Chemical Society*, 2002, **124**, 15267-15279.
26. C. Fressigné, A. Corruble, J.-Y. Valnot, J. Maddaluno and C. Giessner-Prettre, *Journal of Organometallic Chemistry*, 1997, **549**, 81-88.
27. M. Tacke, *European Journal of Inorganic Chemistry*, 1998, **1998**, 537-541.
28. O. A. Vydrov and G. E. Scuseria, *The Journal of Chemical Physics*, 2006, **125**, 234109.
29. J. Tomasi, B. Mennucci and R. Cammi, *Chemical Reviews*, 2005, **105**, 2999-3094.
30. A. V. Marenich, C. J. Cramer and D. G. Truhlar, *The Journal of Physical Chemistry B*, 2009, **113**, 6378-6396.
31. V. Barone and M. Cossi, *The Journal of Physical Chemistry A*, 1998, **102**, 1995-2001.
32. Y. Zhao, N. González-García and D. G. Truhlar, *The Journal of Physical Chemistry A*, 2005, **109**, 2012-2018.

GRAPHICAL ABSTRACT

Leighton Jones and Benjamin J. Whitaker

Modeling a Halogen Dance (HD) Reaction Mechanism: A Density Functional Theory (DFT) Study



A DFT approach reveals the bromide auto-catalysis and pseudo-clock nature of the halogen-dance (HD) mechanism with thiophene. Kinetic and thermodynamic calculations find both four-centre and S_N2 mechanisms; the latter giving barrierless reaction steps. Exploring the lithium-halogen exchange mechanism is critical to understand the complex HD reaction.

Figures and Tables

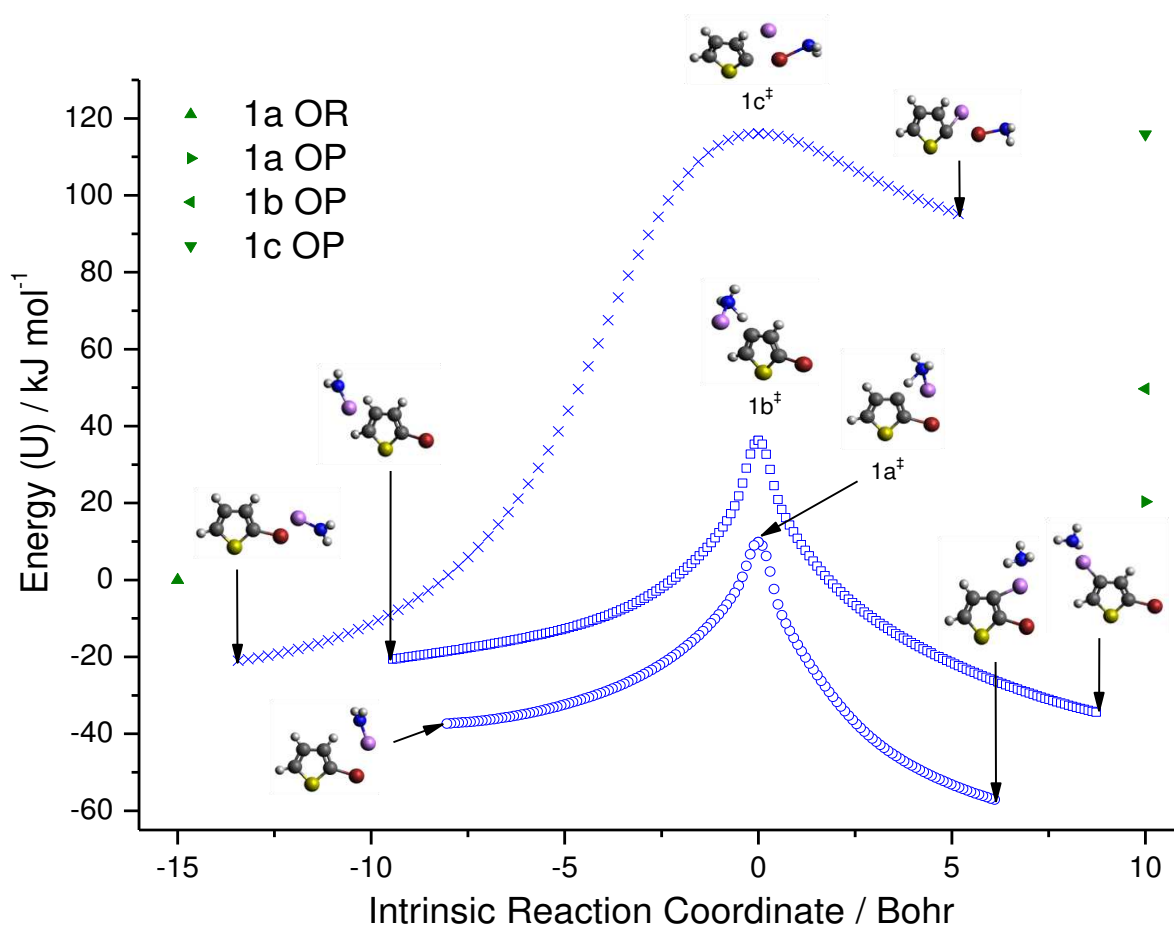
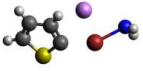


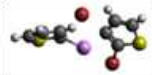
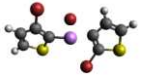
Figure 1.

Table 1. Transition states^a, frequencies, activation energies and Gibbs reaction energies for steps 1a-c.

Step	TS [‡]	Vibration / cm ⁻¹	U _a / kJ mol ⁻¹	Δ _r G / kJ mol ⁻¹
1a		1325 <i>i</i>	9.81	22.51
1b		1366 <i>i</i>	30.26	51.05
1c		229.1 <i>i</i>	110.11	115.53

[a] Computed at the B3LYP/6-311++G(d,p) level.

Table 2. Transition states (four-centre type), frequencies, activation energies and Gibbs reaction energies for steps 2-4.

Step	TS [‡]	Vibration / cm ⁻¹	U _a / kJ mol ⁻¹	Δ _r G / kJ mol ⁻¹
2		265.0 <i>i</i>	202.2	11.05
3		266.2 <i>i</i>	175.6	-49.29
4		272.5 <i>i</i>	193.1	-38.25

[a] Computed at the B3LYP/6-311++G(d,p) level

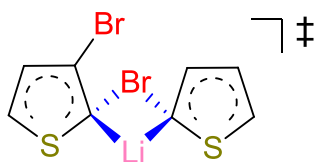
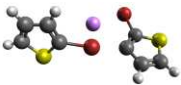
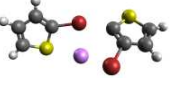


Figure 2.

Table 3. Activation energies (kJ mol ⁻¹) considering explicit and continuum solvation models at the B3LYP-D2/6-311++G(d,p) level.				
Step	THF ^a	IEFPCM ^b	SMD ^c	CPCM ^d
1a	18.59	26.15	18.47	25.96
2	222.9	215.5	195.5	215.1

[a] Explicit THF molecule, [b] the default Integral Equation Formalism Polarizable Continuum Model (IEFPCM) in G09, [c] Truhlar's and co-workers solvation model incorporating electron density (SMD), [d] Conductor Polarizable Continuum Model (CPCM); [a] is at the B3LYP/6-311++G(d,p) and [b-d] is B3LYP-D2/6-311++G(d,p) levels

Table 4. Transition states (S _N 2 type) ^a , frequencies and activation energies for steps 2, 3 and 4.				
Step	TS [‡]	Vibration / cm ⁻¹	U _a / kJ mol ⁻¹	
2		112.7 <i>i</i>	44.93	
3		143.4 <i>i</i>	-12.22	
4		72.35 <i>i</i>	-20.89	

[a] Calculated at the B3LYP-D2/6-311++G(d,p) level.

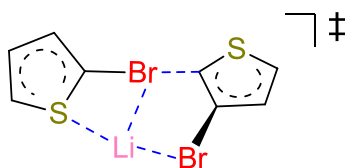


Figure 3.

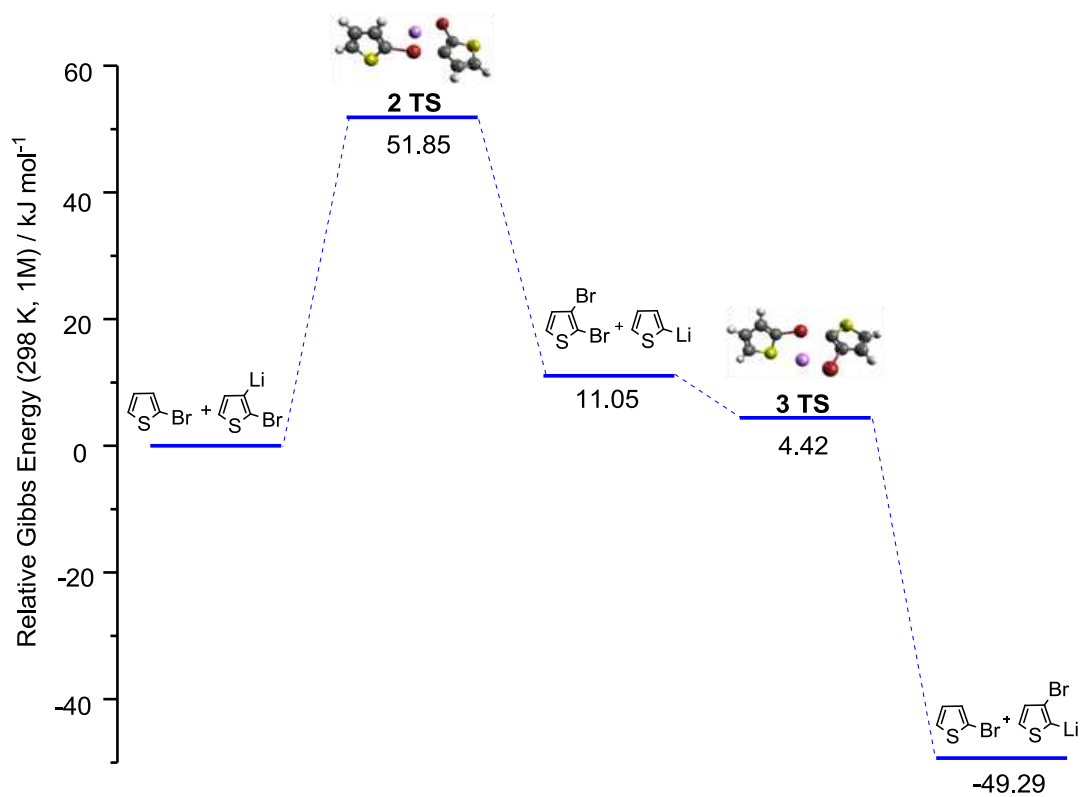


Figure 4.

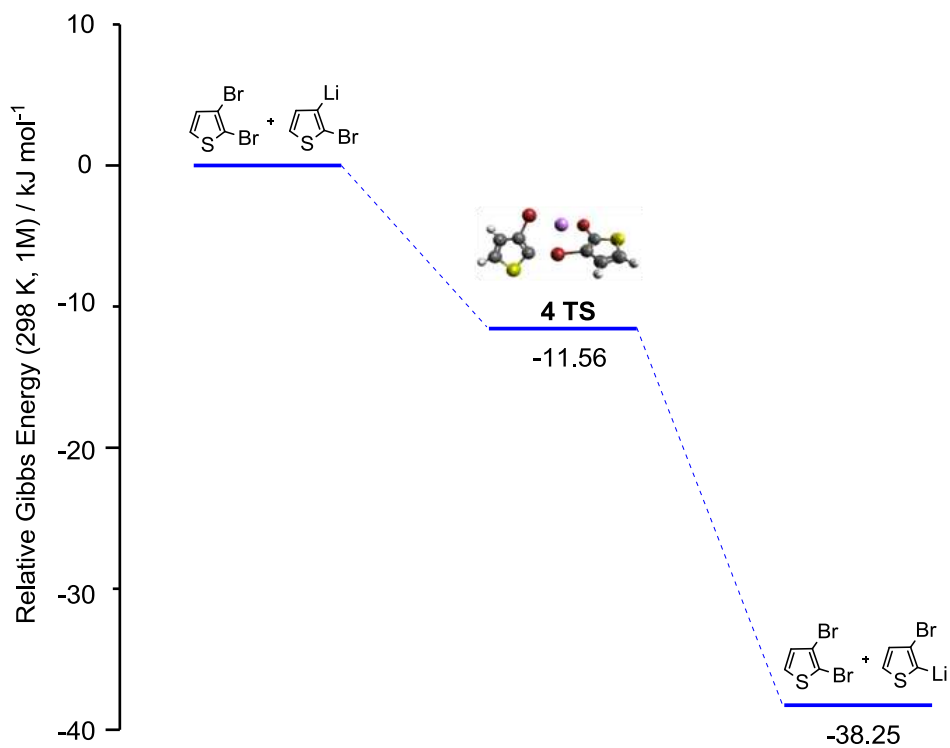
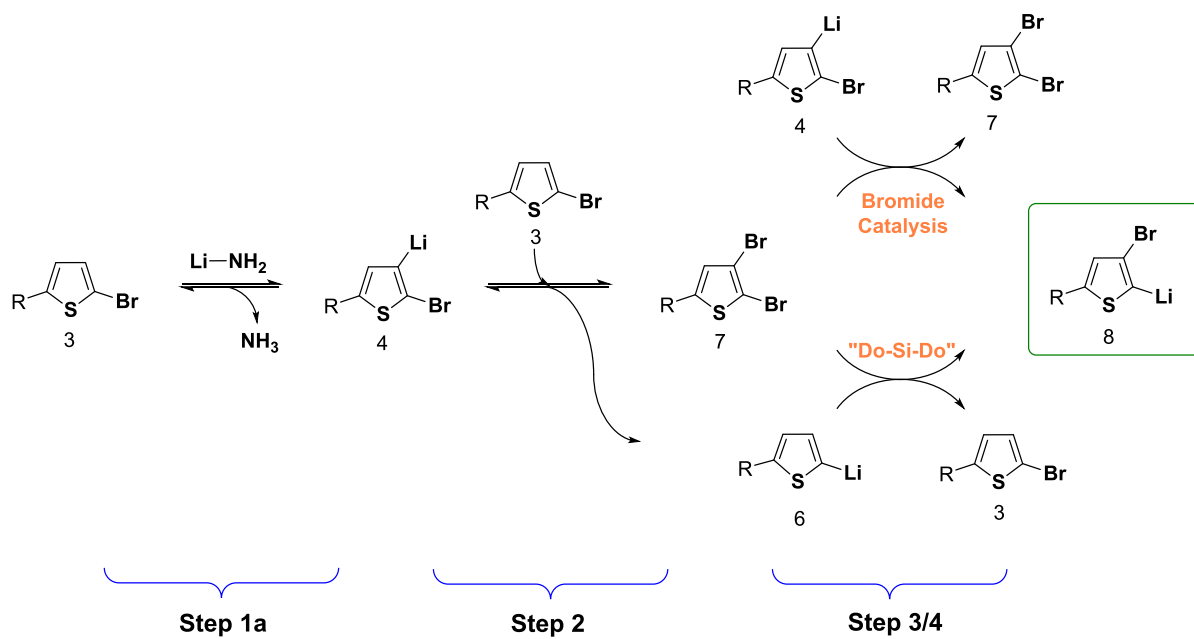


Figure 5.



Scheme 6.